High-fidelity structural loads analysis of the double-swept ERATO rotor

Hyeonsoo Yeo, Mikel Balmaseda, Buvana Jayaraman, Francois Richez, Biel Ortun

HIGH-FIDELITY STRUCTURAL LOADS ANALYSIS OF THE DOUBLE-SWEPT ERATO ROTOR

Hyeonsoo Yeo

U.S. Army Combat Capabilities Development Command
Aviation & Missile Center
Ames Research Center, Moffett Field, CA, USA

Mikel Balmaseda Aguirre

DAAA/ONERA
Institut Polytechnique de Paris
Meudon, France

Buvana Jayaraman

U.S. Army Combat Capabilities Development Command
Aviation & Missile Center
Ames Research Center, Moffett Field, CA, USA

François Richez Biel Ortun

DAAA/ONERA
Institut Polytechnique de Paris
Meudon, France

ABSTRACT

The ERATO rotor wind tunnel test data are investigated to assess the accuracy of analytical tools in the calculation of rotor airloads and structural loads. Comprehensive analysis codes, HOST and RCAS, and coupled computational fluid dynamics/comprehensive analysis codes, elsA/HOST and Helios/RCAS, are used to calculate the ERATO rotor blade dynamics, trim, airloads, and structural loads. The calculated results are compared with the measured data for a high-speed case. RCAS shows excellent correlation with the measured non-rotating blade natural frequencies and the accuracy of the calculated frequencies with RCAS is moderately better than the predictions with HOST. The coupled analyses show improved correlations than the standalone comprehensive analysis for trim, negative lift phase, large pitching moment magnitude on the advancing side and dynamic stall on the retreating side, flap bending and torsion moment phase, and half peak-to-peak flap bending moment. However, the coupled analyses overpredict half peak-to-peak torsion moment and unable to capture 6/rev chord bending moment.

NOTATION

A	rotor disk area, πR^2
a	speed of sound, m/s
c	chord, m
C_L	rotor lift coefficient, $L/\rho(\Omega R)^2 A$
C_X	rotor propulsive force coefficient, $X/\rho(\Omega R)^2 A$
f_m	blade section pitching moment per unit length, Nm/m
f_n	blade section normal force per unit length, N/m
L	rotor lift, N
$M^2 c_m$	blade section pitching moment coefficient times Mach number squared, $f_m/\frac{1}{2}\rho a^2 c^2$
$M^2 c_n$	blade section normal force coefficient times Mach number squared, $f_n/\frac{1}{2}\rho a^2 c$
r	blade radial station, m
R	blade radius, m
V_∞	freestream velocity, m/s
X	rotor propulsive force, N
α_s	shaft angle (positive for rearward tilt), deg
β_{1c}	longitudinal flapping, deg
β_{1s}	lateral flapping, deg
θ_o	collective, deg
θ_{1c}	lateral cyclic, deg
θ_{1s}	longitudinal cyclic, deg
μ	advance ratio, $V_\infty/\Omega R$
ρ	freestream density, kg/m^3
σ	rotor solidity
Ω	rotor angular velocity, rad/s
CBM	chord bending moment
FBM	flap bending moment
TM	torsion moment

Presented at the 50th European Rotorcraft Forum, Marseille, France, September 10-12, 2024.

INTRODUCTION

The rotorcraft community has always been interested in developing advanced rotors which improve performance and reduce vibration and noise. This technology is essential for successful design of future rotorcraft. Modern rotor blades have begun to depart from simple straight planforms by incorporating tip sweep, taper, and anhedral. For example, deviation from the classical rectangular shape in order to significantly reduce noise generated by blades led to the research ERATO (Etude d'un Rotor Aéroacoustique Technologiquement Optimisé) rotor blade.

ERATO is a cooperative research project of French ONERA (Office National d'Etudes et de Recherches

Aérospatiales) and German DLR (German Aerospace Center) with technical advice from Eurocopter (currently Airbus Helicopters) to reduce BVI (blade vortex interaction) noise signature by passive design (Refs. 1–5). The project started in early 1990s. The design optimization study used ONERA 7AD rotor as a baseline geometry. Comprehensive analyses (CA) with vortex wake models and acoustics prediction tools were heavily used for the design process. The project developed ERATO aeroacoustically optimized rotor blade shown in Fig. 1. Some of the design features are briefly described below. Varying the blade chord redistributes the loading along the span and modifies the trailed vorticity. The largest chord of the ERATO blade is located around 65% radius which redistributed lift from the tip towards inboard section and reduced tip vortex strength. BVI noise is generated mainly from unsteady pressure fluctuations on a blade when a blade passes in close proximity to tip vortices from previous blades. A straight blade would experience a parallel interaction with vortex, which normally produces the largest-amplitude impulse noise. The fore-aft sweep of the ERATO blade is beneficial by reducing parallel interaction with vortex. OA3 and OA4-series airfoils used for the ERATO rotor instead of OA2-series airfoils for the 7AD rotor also contributed to the noise reduction and performance improvement.

Once the ERATO blade design was completed, a Mach-scaled model rotor was built and tested in wind tunnel. The wind tunnel tests were conducted in ONERA S1MA (S1 Modane-Avrieux) in the high-speed range (up to 350 km/h) and DNW (German-Dutch Wind Tunnels) in the low to moderate airspeed range (70 to 260 km/h) to verify the design methodology employed. Extensive data were collected on blade deformation, flowfield including tip vortex trajectory, blade surface pressures and section airloads, blade structural loads, rotor forces and moments, and acoustics. The wind tunnel tests demonstrated noise reduction up to 7 dB in descent flight and up to 13 dB at high speed. Significant rotor performance improvement (4 - 12%) was also obtained for low to moderate blade loading. However, hover test conducted by Airbus Helicopters revealed lower figure of merit than the baseline 7AD rotor at high-thrust conditions, most likely because the thin airfoil with small chord near the tip of the blade caused pre-mature stall (Refs. 4, 5).

Based on the success of the ERATO rotor, Airbus Helicopters and ONERA developed a full-scale industrial Blue Edge^{TM} rotor (Refs. 4–7). Extensive design study was performed to improve hover performance and reduce control loads while maintaining low noise characteristics. This was the first time that computational fluid dynamics (CFD) was used by Airbus Helicopters and ONERA for a rotor blade design and optimization. The Blue Edge^{TM} rotor was flight tested successfully on the EC155 Demonstrator and has been incorporated onto the Airbus Helicopters H160.

These programs also emphasize the importance of accurate and robust analytical tools for cost-effective design of modern rotorcraft. Rotorcraft aeromechanics prediction capability using coupled CFD/CA has advanced significantly in recent years (Refs. 8–10). Comprehensive analyses based on multibody finite element modeling solve the complex structural dynamics of nonlinear elastic rotating blades. The CFD methods directly address flow separation, blade stall, three-dimensional unsteady transonic flow as well as the rotor wake flowfield. Coupling a CFD code to a CA code overcomes the limitations of CA codes' conventional lifting line aerodynamic modeling. At convergence of coupled analyses, the CA airloads are completely replaced by the CFD airloads resulting in a consistent, trimmed aeroelastic solution.

This high-fidelity methodology has been extensively used to validate with flight and wind tunnel test data for the UH-60A rotor (Refs. 11–13), 40% Mach-scaled Bo105 main rotor for HART-II (Refs. 14, 15), and ONERA 7A/7AD rotors (Refs. 16–19). However, very few studies have been published on the high-fidelity analysis of ERATO rotor (Refs. 20, 21).

The U.S. Army Combat Capabilities Development Command Aviation & Missile Center (DEVCOM AvMC) and the French ONERA have conducted research to investigate the airloads and structural loads of the ERATO rotor under the auspices of the United States/France Project Agreement on Rotary Wing Aeromechanics and Human Factors Integration Research. The objective of this effort is to accurately predict the ERATO rotor blade loads for various operating conditions using high-fidelity analyses and ultimately demonstrate the suitability of these analysis tools for the design of future rotor blades. The focus of this paper is the ERATO rotor structural dynamics and loads correlation for a high-speed case using both standalone comprehensive analyses and coupled CFD/CA analyses. A companion paper (Ref. 22) by the same authors of the present paper examines rotor performance and airloads.

DESCRIPTION OF THE TEST

The ERATO rotor is a four-bladed fully articulated rotor, with a radius of 2.1 m and solidity, σ, of 0.085. The blade has an advanced planform design with a double-sweep concept. The blade has linear twist for most of the blade span, but nonlinear twist distribution near the tip. The highly-instrumented ERATO rotor was tested in the ONERA S1MA transonic wind tunnel in 1998 (Fig. 2). The ONERA S1MA is a closed circuit atmospheric wind tunnel with a maximum speed near Mach 1, and has three exchangeable test sections with a diameter of 8 m. This wind tunnel test generated an extensive database covering several different speed and thrust conditions. The database provides rotor performance, blade section pressures and airloads, structural loads, and blade motions, allowing for the validation of both aerodynamic and structural models of analytical tools.

Figure 1 shows the blade planform along with the location of the airfoils used. Absolute pressures were measured at five radial locations (50.0%, 75.0%, 85.0%, 92.5%, and 97.5%R). Blade structural loads were obtained from strain gages installed on the blade. Flap bending moments are available at ten radial locations (17%, 23%, 29%, 42.9%, 57%, 71.4%, 76%, 81%, 86%, and 90%R), chord bending moments at four

radial locations (17%, 23%, 57%, and 71.4%R), and torsion moments at seven radial locations (17%, 29%, 57%, 71.4%, 81%, 86%, and 90%R) for the test case investigated in this paper. Both blade pressure data and strain gauge data were collected at a rate of 256 samples/rev (about 1.4° resolution). Both data sets were ensemble averaged over 30 rotor revolutions.

Data from a high-speed wind tunnel test case are used in this study. The high-speed condition ($\mu = 0.423$) is characterized by transonic flow on the advancing side which causes high-vibratory hub loads. The test conditions are listed in Table 1. The rotor was trimmed to the specified rotor lift, propulsive force, and zero one-per-rev flapping ($\beta_{1c} = 0$, $\beta_{1s} = 0$) using rotor collective, lateral and longitudinal cyclics, and shaft angle.

DESCRIPTION OF ANALYTICAL METHODS

The analytical results were obtained using both standalone comprehensive analyses and coupled CFD/CA analyses. ONERA used elsA (Ref. 23) for CFD and HOST (Helicopter Overall Simulation Tool) (Ref. 24) for CA, and the U.S. Army used Helios (HELIcopter Overset Simulations) (Ref. 25) for CFD and RCAS (Rotorcraft Comprehensive Analysis System) (Refs. 26, 27) for CA. Descriptions of each analysis and how they are coupled to produce a higher fidelity solution are provided in this section.

elsA

The elsA CFD code (Ref. 23), developed at ONERA, solves the unsteady Reynolds-Averaged Navier-Stokes (URANS) equations for both background Cartesian grids and blade curvilinear grids. Cartesian grid generation and overset grid assembly is done automatically by the pre- and post-processing tool Cassiopee (Ref. 28). The spatial discretization of the equations is performed with Jameson's cell-centered second order scheme, using 2nd and 4th order coefficients of artificial viscosity. The unsteady algorithm corresponds to a backward Euler scheme, with an implicit Gear scheme for the 2nd-order time integration. The time step is progresively reduced up to 0.25 deg of blade rotation during the 11 coupling iterations. At each time step 30 Newton sub-iterations are used to iteratively solve the nonlinear problem. Turbulence is taken into account by the Kok k-ω model (Ref. 29), with Menter shear stress transport (SST) corrections (Ref. 30) and Zheng limiter (Ref. 31). The flow is modeled as fully turbulent. The near-body grids of the blades are rotated and deformed following the blade motion and trim provided, through the loose coupling, by the rotorcraft comprehensive analysis HOST.

HOST

HOST (Ref. 24) is a rotorcraft comprehensive analysis developed by Airbus Helicopters. HOST modeling of blade dynamics is multibody-like. The blade is represented as an assembly of rigid segments connected by virtual joints. Euler-beam modeling provides 3 degrees of freedom (flapwise bending, chordwise bending, and torsion). A modal reduction approach is used to reduce the number of degrees of freedom from a large system of equations. The aerodynamics of HOST uses a lifting line approach based on airfoil look-up tables combined with a wake model. In this effort, among the several wake models available, a prescribed helical wake was used. For the coupling with elsA, HOST airloads are corrected, via the delta method (Ref. 11), by the CFD airloads.

The ERATO rotor blade structure is modeled in HOST using 34 rigid elements connected by virtual hinges (flap, lag, and torsion). Blade dynamic responses are calculated with eight modes and eight harmonics. Section lift, drag, and moment values for the airfoils are obtained from airfoil look-up tables. Due to proprietary issues, the original airfoil tables used by ONERA were not shared with the U.S. Army. Thus, the airfoil tables are calculated from C81Gen by the U.S. Army. C81Gen is a Navier-Stokes based program that generates an airfoil table in C81 format. C81Gen runs two-dimensional, time-dependent compressible solver ARC2D with structured body fitted viscous gridding. ONERA performed HOST analysis with the two sets of airfoil tables and confirmed that rotor performance and loads agree reasonably well. For the current study, both HOST and RCAS used the C81Gen generated airfoil tables. A 5.0 deg azimuthal step size was used for the structural dynamics and trim calculations in HOST.

Helios

Helios (Ref. 25), developed by the U.S. Army and the Department of Defense Computational Research and Engineering Acquisition Tools and Environments - Air Vehicles (CREATE^{TM}-AV) program, is a multidisciplinary computational platform for high fidelity rotorcraft analysis. Helios uses a multi-mesh, multi-solver paradigm. Near-body solvers such as NASA's OVERFLOW (Ref. 32) structured solver and FUN3D (Ref. 33) unstructured solver, kCFD unstructured solver (Ref. 34), and mStrand multi-strand solver (Ref. 35) are integrated in Helios to capture the wall-bounded viscous effects. Cartesian grids in the off-body are used to resolve the wake through a combination of higher-order algorithms and adaptive mesh refinement (AMR). The Cartesian off-body grids are solved with SAMCart using a 5th-order central difference scheme in space and either a 3rd-order explicit 3-stage Runge-Kutta scheme or 2nd-order implicit lower-upper symmetric-Gauss-Seidel method (LU-SGS) BDF2 in time. An overset procedure is used to facilitate data exchange; it also enables relative motion between meshes using the parallel domain connectivity solver PUNDIT (Parallel UNsteady Domain Information Transfer). Helios also has the ability to perform CFD/CA coupling using the comprehensive analysis codes RCAS and CAMRAD II (Ref. 36) which allows the blades to be trimmed throughout the course of these simulations.

In this effort Helios solves the near-body grids around the rotor blades and test stand with the CFD solver OVERFLOW, using a 5th-order central difference scheme in space and a 2nd-order backward differentiation formula (BDF2) scheme in time. The fully turbulent flow is modeled using the Spalart-Allmaras delayed detached eddy simulation (SA-DDES) turbulence model in both the near- and off-body grids. The time step is equivalent to an azimuthal step size of 0.25 deg. AMR was not used.

RCAS

RCAS (Refs. 26, 27) is a comprehensive analysis developed by the U.S. Army to provide state-of-the-art rotorcraft modeling and analysis technology for Government, industry, and academia. It is a multi-disciplinary software system capable of detailed modeling a wide range of rotorcraft configurations operating in hover, forward flight, and maneuvering flight to predict performance, loads, vibration, flight dynamics, and aeroelastic stability.

The ERATO rotor blade is modeled in RCAS using 18 nonlinear beam elements and 28 aerodynamic segments. As mentioned, both HOST and RCAS use the same airfoil tables generated by the U.S. Army. The rotor hub was modeled as fully articulated with pitch bearing and flap and lag hinges. The elastomeric lag damper of the ERATO rotor was modeled with equivalent hinge stiffness and damping values at the lag hinge. A 5.0 deg (72 steps per rotor revolution) azimuthal step size was used for the structural dynamic calculations in RCAS. The RCAS standalone analysis was conducted using nonuniform inflow with prescribed wake geometry and unsteady aerodynamics based on classical quasi-steady Theodorsen theory (Ref. 37).

CFD/CA coupled analysis

The CFD/CA coupling procedure used the standard loose or "delta" coupling approach (Ref. 11). At each coupling iteration the aerodynamic loads calculated by CFD are passed to CA. After trimming with the CFD airloads, CA computes the blade deflections and passes them back to CFD. This sequence is repeated until the airloads, deflections, and control angles converge. The trim parameters used in the predictions are the same as those from the test, a four degree-of-freedom trim. The trim targets are the specified rotor lift, rotor propulsive force and zero first harmonic flapping.

Both elsA and Helios CFD codes use overlapping grids consisting of structured curvilinear near-body grids rotating in a Cartesian background grid. All the CFD simulations considered in this work are assumed to be fully turbulent (i.e., no laminar-to-turbulent transition effects are modeled). The computational grids model the ERATO rotor blade geometry and test stand, but do not include a hub or the wind tunnel walls.

The size of the elsA grid shown in Fig. 3(a) is approximately 32.7M points: 5.5M points for blade body-fitted grids, 1M points for test stand, and 26.2M points for Octree background grid. The minimum grid size of the background mesh is approximately 9% of the main chord (0.14 m). For Helios, shown in Fig. 3(b), fully structured overset solver OVERFLOW was used for the ERATO blades. Each blade grid has approximately 13M nodes and the stand grid has approximately 1.6M nodes. In the off-body, 8 levels of grid are used with fixed refinement regions around the blade and test stand with a total of 757M nodes. For these regions, the finest grid spacing is approximately 6% of the tip chord.

In the HOST and elsA/HOST analyses, the blade is represented by the first eight eigenmodes and the blade periodic response was calculated with up to eight harmonics. For the RCAS and Helios/RCAS analyses, full finite element representation of the blade is maintained throughout the dynamic analysis and no harmonic truncation is used. Neither comprehensive analysis included blade structural damping, test stand dynamics, or drivetrain dynamics. Previous study showed that test stand and drivetrain dynamics for this test apparatus did not appear to play a significant role for rotor loads correlation (Ref. 19).

RESULTS AND DISCUSSION

In this section, selected data from the wind tunnel test are compared with predictions from two comprehensive analyses (HOST and RCAS) and two coupled analyses (elsA/HOST and Helios/RCAS). These test data include blade frequencies, trim angles, blade section airloads, and blade structural loads for the high-speed case.

Rotor blade dynamics

ERATO rotor structural dynamics models were developed using HOST and RCAS comprehensive analysis codes. And then, non-rotating blade natural frequencies are calculated and the analysis results are compared with experimental measurements in Table 2. Comparisons are made for up to seven modes, which include four flap modes, two lag modes, and one torsion mode.

In the shake test, the blade was positioned vertically as shown in Fig. 4. The blade is connected to the root fixture at the twin pin location (0.275 m). A thin metallic plate was located at 0.075m to simulate the flap hinge. The parts between the root and the thin metallic plate and between the thin metallic plate and the twin pins are rigid. Although the thin metallic plate was designed to simulate only flap hinge, it was not perfectly rigid in the lag direction. A lag hinge and spring were introduced at 0.075m to simulate flexibility in the lag direction and spring stiffness was tuned to match with the measured first lag frequency. And then, the calculated second lag frequency is compared against the measured value to evaluate the accuracy of the model.

In general, RCAS shows excellent correlation with the measured data. Accuracy of the calculated frequencies with RCAS is moderately better than the predictions with HOST.

HOST tends to underpredict flap and second lag frequencies and overpredict torsion frequency. The fact that the calculated non-rotating frequencies agreed closely with the measured values suggested that the blade properties were properly defined and the analyses accurately modeled the ERATO rotor blade structural dynamics.

Figure 5 compares calculated blade natural frequencies in vacuum as a function of normalized rotor speed. Measured rotating blade modal data are not available and thus, frequency correlation could not be conducted. The frequencies shown here are for a nominal zero collective pitch. There is significant flap-torsion coupling due to double-swept blade planform. Frequency predictions by the two comprehensive codes show very good agreement for low-frequency modes, however, differences are shown for higher frequency modes. Similar to the non-rotating frequency comparison, flap and lag frequencies calculated with HOST are lower than those with RCAS and torsion frequency calculated with HOST is higher than that with RCAS.

Trim angles

Figure 6 shows the calculated and measured blade pitch angles and shaft angle. HOST and elsA/HOST results are compared in Fig. 6(a), and RCAS and Helios/RCAS results are compared in Fig. 6(b). The coupled analysis results shown here include the test stand modeling. HOST shows reasonably good agreement of the measured shaft angle, but underpredicts blade pitch angles. This is especially true for lateral cyclic angle, which was underpredicted by about 3.2 deg. The coupled elsA/HOST analysis shows better agreement with the measured blade pitch and shaft angles, with lateral cyclic angle difference around 0.9 deg. Similar improvement is obtained with the coupled Helios/RCAS analysis compared to the RCAS standalone analysis.

Effects of test stand on rotor trim was investigated in Ref. 18 with ONERA 7A rotor installed on the same test stand as the present ERATO rotor test in the same S1MA wind tunnel using the same analysis tools. Adding the test stand significantly improved the agreement with the experimentally measured lateral cyclic angle, which increased to counter the test stand upflow through the front of the rotor disk and downflow over the back of the rotor disk.

There is, in general, good agreement between the two comprehensive analyses and between the two coupled analyses. The only difference is that the shaft angle correlation was not improved with the coupled Helios/RCAS analysis compared to the RCAS standalone analysis.

Airloads

Blade section normal force and pitching moment are briefly examined in this section. More detailed pressure and airloads comparisons are available in Ref. 22. A visualization of the vortex wake structure behind the ERATO rotor is shown in Fig. 7. The wake is quickly convected from the rotor disk in high speed condition. This figure illustrates chaotic wake structure induced by the wind tunnel test stand. Figure 8 shows non-dimensional normal force at 85%R and 97.5%R and pitching moment at 97.5%R. To obtain section airloads from CFD, calculated blade pressures are integrated. The number of points used to integrate the measured pressure data (i.e., the number of pressure transducers) is much less than the grid points used for the CFD calculations. For comparison with measured data, integration of the CFD-calculated pressures were made at the same pressure transducer locations used in the measurements. For the comprehensive analyses based on lifting-line aerodynamics and airfoil tables, blade section airloads are calculated from airfoil section lift, drag and moment values based on the local section angle-of-attack and Mach number, and thus there is no integration of pressure involved. The test stand model cannot be included in the comprehensive analyses, either.

The rotor blade aerodynamic environment at high speed is characterized by compressibility, and negative lift and large aerodynamic pitching moment on the advancing side. For the normal force comparison, the standalone comprehensive analyses show reasonably good correlation on magnitude, but the phase correlation is poor, which is a typical limitation of comprehensive analyses based on lifting-line aerodynamics. The coupled analyses significantly improve the phase of the negative lift and waveform in the first quadrant. A large aerodynamic pitching moment on the advancing side is also better captured by the coupled analyses.

It is interesting to note significantly large negative pitching moment on the retreating side due to dynamic stall. Normally dynamic stall occurs at high-thrust conditions. For example, ONERA 7A rotor showed no signs of dynamic stall at a high-speed condition ($\mu = 0.4$, $C_L/\sigma = 0.063$), but showed dynamic stall at a high-thrust condition ($\mu = 0.3$, $C_L/\sigma = 0.100$) (Ref. 18). As mentioned earlier, the thin airfoil with small chord near the tip of the ERATO rotor blade is related to this dynamic stall. The coupled analyses also capture beginning of dynamic stall very well, but the extent of the calculated stall regions is wider than the test data.

Structural loads

This section compares the calculated blade flap bending, chord bending, and torsion moments with the wind tunnel test data. Time history results at three radial locations are compared first, and then half peak-to-peak magnitude will be compared along the blade span, and finally detailed harmonic components are compared.

Figure 9 shows oscillatory flap bending moment at 17%R, 57%R, and 76%R. Steady values were removed from both test data and analyses. The measured data show that a 2/rev harmonic is dominant, which appears to be primarily affected by the second flap mode whose predicted frequency is about 2.4/rev. The comprehensive analyses show significant phase differences, similar to the normal force correlation shown in Fig. 8. The coupled analyses show better correlation with the

test data. Waveform and phase correlation is substantially improved at all azimuth angles by the coupled analyses. Peak-to-peak magnitudes are also better predicted by the coupled analyses.

Figure 10 shows oscillatory torsion moments at 17%R, 57%R, and 76%R. The measured torsion moments show strong 4 and 5/rev content. Both comprehensive analyses overpredict the peak-to-peak magnitudes and show significant phase differences. The coupled analyses improve phase in the first and second quadrants. However, elsA/HOST significantly overpredicts peak-to-peak magnitude and Helios/RCAS is not able to capture high-frequency content.

Figure 11 shows oscillatory chord bending moments at 17%R, 57%R, and 71.4%R. The measured data show that a 6/rev harmonic is dominant, which appears to be primarily affected by the second lag mode whose predicted frequency is close to 6/rev. HOST analysis shows significant phase differences and tends to underpredict the magnitude. elsA/HOST analysis improves phase correlation and better captures high-frequency content. However, peak-to-peak magnitude is still underpredicted. RCAS analysis captures high-frequency content very well, but there are phase differences. Helios/RCAS analysis is not able to capture high-frequency content, although the same structural dynamics model was used for both RCAS and Helios/RCAS analyses. This needs further investigation.

Figure 12 shows comparisons between analytical predictions and measured data for half peak-to-peak values of the blade structural loads. Half peak-to-peak values of flap bending moment are plotted in Figs. 12(a) and 12(b) as a function of the radial position. The measured data show that half peak-to-peak flap bending moment has a peak near the blade root (17%R), decreases from blade root to 29%R, and increases to a local peak around 57%R before it decreases further outboard. All the analyses also exhibit similar behavior, but with some deficiencies. In general, predictions with comprehensive analyses are much lower than the measured data. elsA/HOST predictions, in general, show good agreement with the test data, except for the blade root location (17%R). Helios/RCAS shows good correlation near the blade root (17%R to 29%R), but shows significant underprediction near the midspan. Figures 12(c) and 12(d) show the half peak-to-peak values for torsion moment. The measured data show a peak at 29%R and decrease to the blade tip. Both comprehensive analyses overpredict the half peak-to-peak magnitudes at all data points. As the predicted peak values continue from blade root to midspan, there is substantial overprediction at the midspan. elsA/HOST analysis further increases half peak-to-peak magnitudes and exacerbates the correlation. Helios/RCAS reduces half peak-to-peak magnitudes near the blade root and thus improves correlation. However, overprediction at the midspan remains. Half peak-to-peak chord bending moment is plotted in Figs. 12(e) and 12(f). In general, the measured values decrease continually from blade root to tip, and this trend is reasonably well captured by the analyses. Both HOST and elsA/HOST predictions are lower than the measured data. RCAS shows very good agreement with the test data. Helios/RCAS shows reasonably good correlation, although detailed harmonic analysis (shown later) reveals some deficiencies.

Figure 13 compares harmonic content of flap bending moments along the blade span. Up to 5/rev harmonic components are plotted. Higher frequencies tend to have a smaller amplitude than lower frequencies. For a 4-bladed rotor, 3, 4, and 5/rev blade loads contribute to 4/rev vibratory hub loads and airframe vibration. The test data show strong 1 and 2/rev content. Maximum 1 and 2/rev harmonics occur at 57%R and the analyses capture this trend reasonably well. Coupled analyses increase 2 and 3/rev harmonic magnitudes and improve correlation. Figure 14 compares harmonic content of torsion moments along the blade span. Similar to the flap bending moment, maximum 1 and 2/rev harmonics occur at 57%R and the analyses capture this trend reasonably well. However, the coupled analyses increase 2/rev harmonic magnitude compared to the comprehensive analyses and make the correlation worse. All the analyses also overpredict 3/rev magnitude. Figures 15 and 16 compare harmonic content of chord bending moments along the blade span. Unlike flap bending and torsion moments, the measured data show that a 6/rev harmonic is dominant and a 7/rev harmonic is also strong. HOST, elsA/HOST, and Helios/RCAS substantially underpredict 6/rev harmonic magnitude. Only RCAS is able to capture 6/rev magnitude very well. Helios/RCAS showed good half peak-to-peak correlation with the test data, as shown in Fig. 12(f), because of overprediction of 3/rev harmonic compensated underprediction of 6/rev harmonic. Although the same structural dynamics model was used for both RCAS and Helios/RCAS analyses, there is a significant difference in the chordwise bending moment and this needs further investigation.

SUMMARY AND CONCLUSIONS

The ERATO rotor wind tunnel test data are investigated to assess the accuracy of analytical tools in the calculation of rotor airloads and structural loads at a high-speed condition. Two comprehensive analysis codes, HOST and RCAS, and two coupled computational fluid dynamics/comprehensive analysis codes, elsA/HOST and Helios/RCAS, are used to examine the ERATO rotor blade dynamics, trim, airloads, and structural loads, and the calculated results are compared with the measured data. From this study, the following conclusions are obtained:

1) Non-rotating blade frequencies are calculated using HOST and RCAS, and the analysis results are compared with experimental measurements to evaluate the accuracy of the structural dynamics model. RCAS shows excellent correlation with the measured data and the accuracy of the calculated frequencies with RCAS is moderately better than the predictions with HOST.

For the rotating frequency comparison, the predictions by the two comprehensive codes display very good agreement for low-frequency modes, however, differences are shown for

higher frequency modes. There is significant flap-torsion coupling due to double-swept blade planform.

2) Trim angles (blade pitch angles and shaft angle) are compared between the analyses and the measured data. Comprehensive analyses tend to underpredict blade pitch angles. Coupled analyses, which include the test stand modeling, increase blade pitch angles and improve overall correlation. Improvement of lateral cyclic angle correlations is especially notable.

3) The rotor blade aerodynamic environment at high speed is characterized by compressibility, and negative lift and large aerodynamic pitching moment on the advancing side. For the ERATO rotor, dynamic stall is also observed on the retreating side due to the thin airfoil and the reduced chord length at the blade tip.

For the normal force comparison, the standalone comprehensive analyses show reasonably good correlation on magnitude, but the phase correlation is poor. The coupled analyses significantly improve the phase of the negative lift and waveform in the first quadrant. A large aerodynamic pitching moment on the advancing side and dynamic stall on the retreating side are also better captured by the coupled analyses than the comprehensive analyses based on lifting-line aerodynamics.

4) Comprehensive analyses show significant phase differences for the structural loads. The phase correlation is substantially improved by the coupled analyses for the flap bending and torsion moments.

5) The coupled analyses improve the half peak-to-peak flap bending moment correlation compared to the comprehensive analyses by significantly improving 2/rev harmonic magnitude correlation. However, the coupled analyses, in general, overpredict the half peak-to-peak magnitude of torsion moment.

6) The measured chord bending moment data show a dominant 6/rev harmonic magnitude, which appears to be primarily affected by the second lag mode. Only RCAS is able to capture 6/rev magnitude very well. Although the same structural dynamics model was used for both RCAS and Helios/RCAS analyses, there is a significant difference in the chordwise bending moment between the two analyses and this needs further investigation.

ACKNOWLEDGMENTS

The authors would like to acknowledge the U.S./France Project Agreement on Rotary-Wing Aeromechanics and Human Factors Integration Research, a longstanding cooperation between the U.S. Army, ONERA, and DGA.

REFERENCES

[1]Prieur, J., and Splettstoesser, W. R., "ERATO – an ONERA-DLR Cooperative Programme on Aeroacoustic Rotor Optimisation," 25th European Rotorcraft Forum, Rome, Italy, September 14-16, 1999.

[2]Splettstoesser, W. R., Van der Wall, B., Junker, B., Schultz, K. J., Beaumier, P., Delrieux, Y., Leconte, P., and Crozier, P., "The ERATO Programme: Wind Tunnel Test Results and Proof of Design for an Aeroacoustically Optimised Rotor," 25th European Rotorcraft Forum, Rome, Italy, September 14-16, 1999.

[3]Delrieux, Y., Prieur, J., Costes, M., Gardarein, P., Beaumier, P., des Rochettes, H. M., Leconte, P., Crozier, P., Splettstoesser, W. R., van der Wall, B. G., Junker, B., Schultz, K. J., Mercker, E., Pengel, K., Philippe, J. J., and Gmelin, B., "The ONERA-DLR Aeroacoustic Rotor Optimisation Programme ERATO: Methodology and Achieve ments," American Helicopter Society Aerodynamics, Acoustics, and Test and Evaluation Technical Specialists Meeting, San Francisco, CA, January 23-25, 2002.

[4]Van der Wall, B., Kessler, C., Delrieux, Y., Beaumier, P., Gervais, M., Hirsche, J. F., Pengel, K., and Crozier, P., "From ERATO Basic Research to the Blue Edge™ Rotor Blade," AHS 72nd Annual Forum, West Palm Beach, Florida, May 1719, 2016.

[5]Beaumier, P., Kessler, C., Delrieux, Y., Van der Wall, B., Gervais, M., Hirsche, J. F., Pengel, K., and Crozier, P., "From ERATO Basic Research to the Blue Edge™ Rotor Blade: an Example of Virtual Engineering?," Rotorcraft Virtual Engineering Conference, Liverpool, United Kingdom, November 8-10, 2016.

[6]Rauch, P., Gervais, M., Cranga, P., Baud, A., Hirsch, J-F., Walter, A., and Beaumier, P., "Blue Edge™: The Design, Development and Testing of a New Blade Concept," American Helicopter Society 67th Annual Forum, Virginia Beach, VA, May 3-5, 2011.

[7]Gervais, M., and Gareton, V., "Analysis of Main Rotor Noise Reduction Due to Novel Planform Design the Blue Edge™ Blade," 37th European Rotorcraft Forum, Gallarate, Italy, September 13-15, 2011.

[8]Datta, A., Nixon, M., and Chopra, I., "Review of Rotor Loads Prediction with the Emergence of Rotorcraft CFD," *Journal of the American Helicopter Society*, Vol. 52, (4), October 2007, pp. 287-317.

[9]Yeo, H., and Ormiston, R. A., "UH-60A Airloads Workshop – Setting the Stage for the Rotorcraft CFD/CSD Revolution, Part I: Background and Initial Success," *Journal of the American Helicopter Society*, **67**, 022010 (2022).

[10]Yeo, H., and Ormiston, R. A., "UH-60A Airloads Workshop – Setting the Stage for the Rotorcraft CFD/CSD Revolution, Part II: Ongoing Progress, Impact, and Lessons Learned," *Journal of the American Helicopter Society*, **67**, 022011 (2022).

[11]Potsdam, M., Yeo, H., and Johnson, W., "Rotor Airloads Prediction Using Loose Aerodynamic/Structural Coupling," *Journal of Aircraft*, Vol. 43, (3), May-June 2006.

[12]Biedron, R. T., and Lee-Rausch, E. M., "An Examination of Unsteady Airloads on a UH-60A Rotor: Computation versus Measurement," American Helicopter Society 68th Annual Forum Proceedings, Forth Worth, TX, May 1-3, 2012.

[13]Yeo, H., and Potsdam, M., "Rotor Structural Loads Analysis Using Coupled Computational Fluid Dynamics/Computational Structural Dynamics," *Journal of Aircraft*, Vol. 53, (1), JanuaryFebruary 2016.

[14]Boyd Jr., D. D., "HART-II Acoustic Predictions using a Coupled CFD/CSD Method," American Helicopter Society 65th Annual Forum Proceedings, Grapevine, TX, May 27-29, 2009.

[15]Smith, M. J., Lim, J. W., van der Wall, B. G., Baeder, J. D., Biedron, R. T., Boyd, D. D., Jr., Jayaraman, B., Jung, S. N., and Min, B. Y., "The HART II International Workshop: an Assessment of the State of the Art in CFD/CSD Prediction," *CEAS Aeronautical Journal*, Vol. 4, (4), December 2013, pp. 345-372.

[16]Rodriguez, B., Benoit. C., and Gardarein P., "Unsteady Computations of the Flowfield around a Helicopter Rotor with Model Support," Paper AIAA 2005-466, 43rd AIAA Aerospace Sciences Meeting and Exhibit, Reno, NV, January 10-13, 2005.

[17]Pahlke, K., and van der Wall, B. G., "Chimera Simulations of Multibladed Rotors in High-Speed Forward Flight with Weak Fluid-Structure Coupling," *Aerospace Science and Technology*, Vol. 9, (5), July 2005.

[18]Ortun, B., Potsdam, M., Yeo, H., and Truong, V. K., "Rotor Loads Prediction on the ONERA 7A Rotor using Loose Fluid/Structure Coupling," *Journal of the American Helicopter Society*, **62**, 032005 (2017).

[19]Yeo, H., Potsdam, M., Ortun, B., and Truong, K. V., "High-Fidelity Structural Loads Analysis of the ONERA 7A Rotor," *Journal of Aircraft*, Vol. 54, (5), September-October 2017.

[20]Truong, V. K., "Dynamics Studies of the ERATO Blade, Based on Finite Element Analysis," 31st European Rotorcraft Forum, Florence, Italy, September 13-15, 2005.

[21]Ortun, B., Petot, D., Truong, V. K., and Ohayon, R., "Towards a new generation of rotorcraft comprehensive analysis; coupling with CSM and CFD," 34th European Rotorcraft Forum, Liverpool, United Kingdom, September 16-18, 2008.

[22]Balmaseda, M., Yeo, H., Richez, F., Jayaraman, B., and Ortun, B., "High-Fidelity Aerodynamic Loads Analysis of the Double-Swept ERATO Rotor," 50th European Rotorcraft Forum, Marseille, France, September 10-12, 2024.

[23]Cambier, L., Gazaix, M., Heib, S., Plot, S., Poinot, M., Veuillot, J. P., Boussuge, J. F., and Montagnac, M., "An Overview of the Multi-Purpose elsA Flow Solver," *AerospaceLab*, Issue 2, March 2011.

[24]Dequin, A. M., Benoit, B., Kampa, K., von Grünhagen, W., Basset, P. M., and Gimonet, B., "HOST, a General Helicopter Simulation Tool for Germany and France," American Helicopter Society 56th Annual Forum, Virginia Beach, VA, May 2-4, 2000.

[25]Wissink, A. M., Dylan, P. J., Jayaraman B., Roget, B., Lakshminarayan, V. K., Sitaraman, J., Bauer, A. C., Forsythe, J. R., and Trigg, R., "New Capabilities in CREATE^{TM}-AV Helios Version 11," AIAA 2021-0235, Proceedings of the AIAA SciTech 2021 Forum, January 11-15 and 19-21, 2021.

[26]Saberi, H., Hasbun, M., Hong, J. Y., Yeo, H., and Ormiston, R. A., "Overview of RCAS Capabilities, Validations, and Rotorcraft Applications," American Helicopter Society 71st Annual Forum, Virginia Beach, VA, May 5-7, 2015.

[27]Hasbun, M., Saberi, H., and Yeo, H., "Overview of RCAS Capabilities and Validations for Rotorcraft and eVTOL Applications," Vertical Flight Society 80th Annual Forum & Technology Display, Montréal, Canada, May 7-9, 2024.

[28]Benoit, C., Péron, S., and Landier, S., "Cassiopee: A CFD pre- and post-processing tool," *Aerospace Science and Technology*, Vol. 45, 2015, pp. 272-283.

[29]Kok, J. C., "Resolving the Dependence on Freestream Values for the k-ω Turbulence Model," *AIAA Journal*, Vol. 38, (7), July 2000, pp. 1292-1295.

[30]Menter, F. R., "Two-Equation Eddy-Viscosity Transport Turbulence Model for Engineering Applications," *AIAA Journal*, Vol. 32, 1994, pp. 1598-1605.

[31]Zheng, X., Liao, C., Liu, C., Sung, C. H., and Huang, T. T., "Multigrid Computation of Incompressible Flows using Two-Equation Turbulence Models," *Journal of Fluid Engineering*, Vol. 119, 1997, pp. 893-905.

[32]Nichols, R. H., and Buning, P. G., "OVERFLOW User's Manual, Version 2.2," NASA Langley Research Center, Hampton, VA, August 2010.

[33]Biedron, R. T., Jan-Reneé, C., Derlaga, J. M, Gnoffo, P. A, Hammond, D. P, Jones, W. T, Kleb, B., Lee-Rausch, E. M, Nielsen, E. J., Park, M. A., Rumsey, C. L., Thomas, J. L., and Wood, W. A., "FUN3D Manual: 13.3," NASA/TM-2018-219808, NASA Langley Research Center, Hampton, VA, August 2010.

[34]McDaniel, D. R., Tuckey, T. R., and Morton, S. A., "The HPCMP CREATE^{TM}-AV Kestrel Computational Environment and its Relation to NASAs CFD Vision 2030," AIAA 2017-0813, 55th AIAA Aerospace Sciences Meeting, Grapevine, Texas, January 9-13, 2017.

[35]Sitaraman, J., Lakshminarayan, V. K., Roget, B., and Wissink, A. M., "Progress in Strand Mesh Generation and Domain Connectivity for Dual-Mesh CFD simulations," AIAA 2017-0288, 55th AIAA Aerospace Sciences Meeting, Grapevine, Texas, January 9-13, 2017.

[36]Johnson, W., "Technology Drivers in the Development of CAMRAD II," American Helicopter Society Aeromechanics Specialist Meeting, San Francisco, CA, January 1994.

[37]Theodorsen, T., "General Theory of Aerodynamic Instability and the Mechanism of Flutter," NACA Report 496, January 1949.

Table 1. ERATO rotor test conditions

Parameter	High-speed (d630)
Density, kg/m^3	1.051
Temperature, °C	11.0
Rotor speed, rpm	946.0
Airspeed, m/s	88.0
Advance ratio, μ	0.423
Rotor lift coefficient to solidity ratio, C_L/σ	0.063
Rotor propulsive force coefficient to solidity ratio, C_X/σ	0.0091

Table 2. Non-rotating blade frequency comparison

Mode	Measured, Hz	HOST, Hz	RCAS, Hz
Flap 1	14.56	13.82	14.55
Lag 1	21.51	21.44	21.57
Flap 2	42.38	38.00	41.67
Flap 3	71.03	63.86	70.71
Torsion	108.01	113.60	109.76
Flap 4	139.04	122.29	131.35
Lag 2	141.03	130.73	139.91

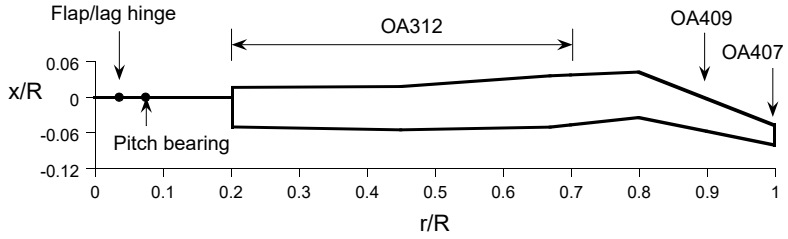

Fig. 1. ERATO rotor planform (Refs. 4, 5)

Fig. 2. ERATO rotor mounted in the ONERA Modane S1MA Wind Tunnel.

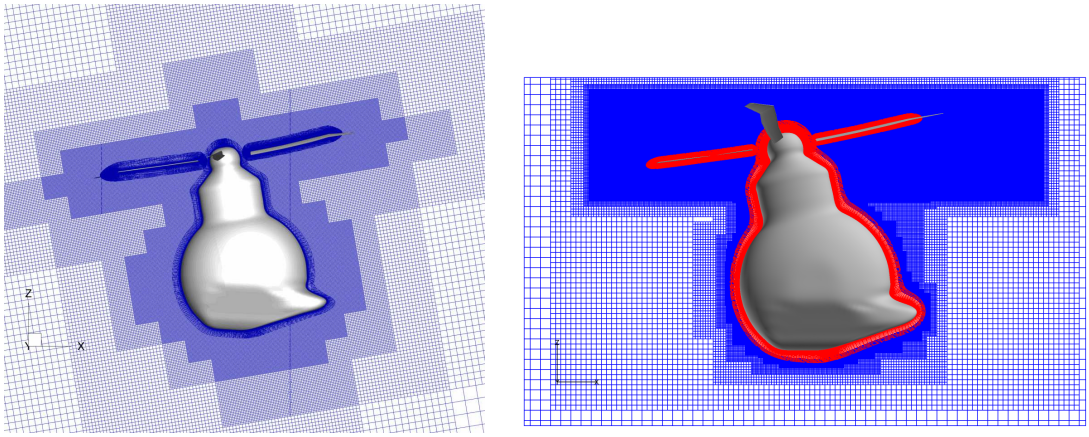

(a) elsA (b) Helios

Fig. 3. Overset grid systems.

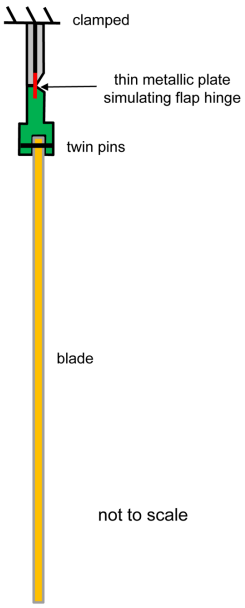

Fig. 4. Nonrotating blade frequency test setup.

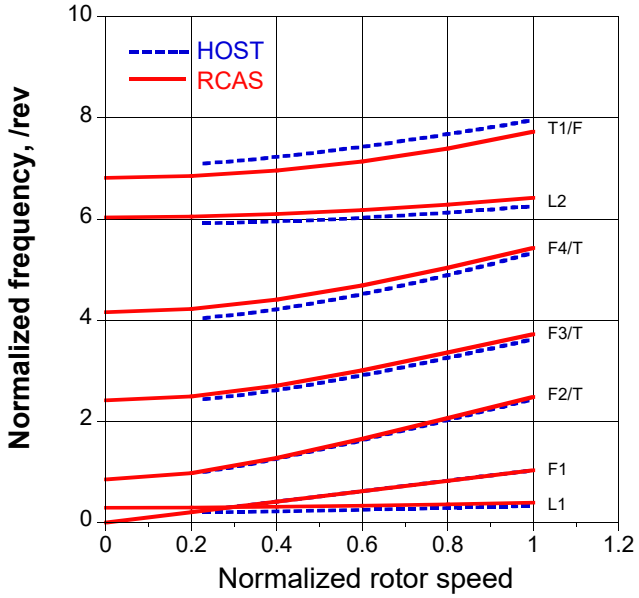

Fig. 5. Rotating blade frequency comparison.

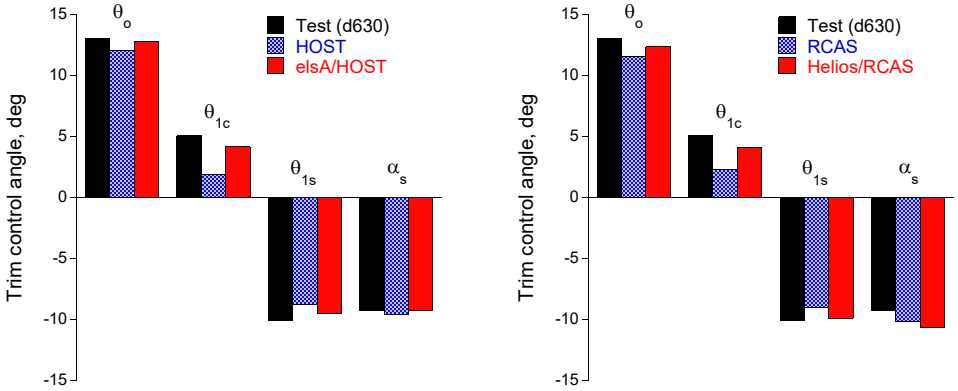

(a) HOST and elsA/HOST

(b) RCAS and Helios/RCAS

Fig. 6. Trim control angles.

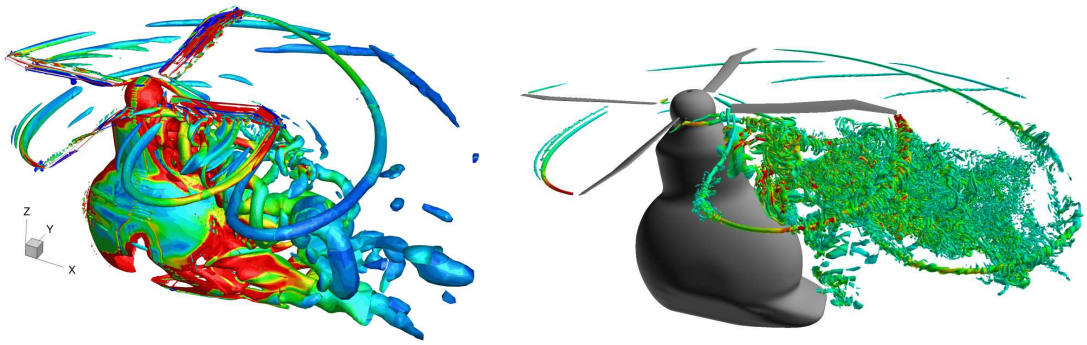

(a) elsA (b) Helios

Fig. 7. Isocontours of Q-criterion in the wake of the ERATO rotor.

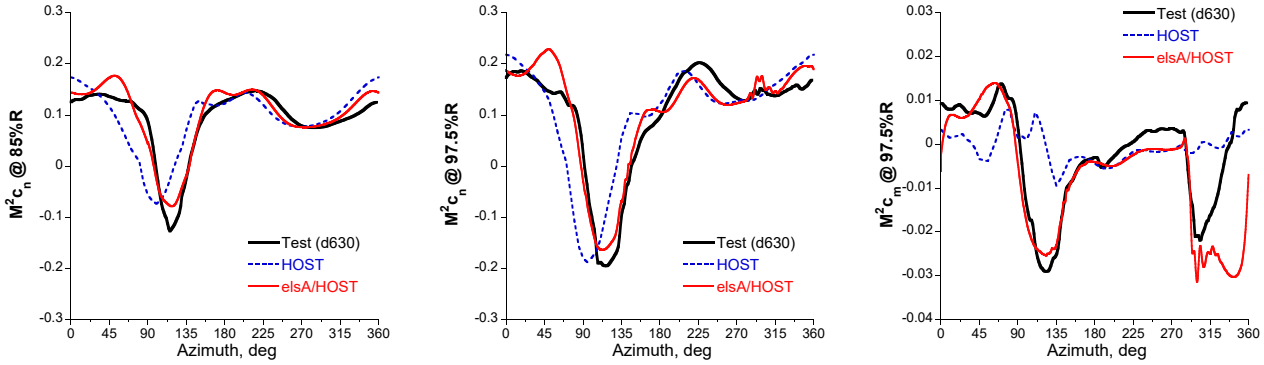

(a) Normal force at 85%R (b) Normal force at 97.5%R (c) Pitching moment at 97.5%R

(d) Normal force at 85%R (e) Normal force at 97.5%R (f) Pitching moment at 97.5%R

Fig. 8. Blade normal force and pitching moment.

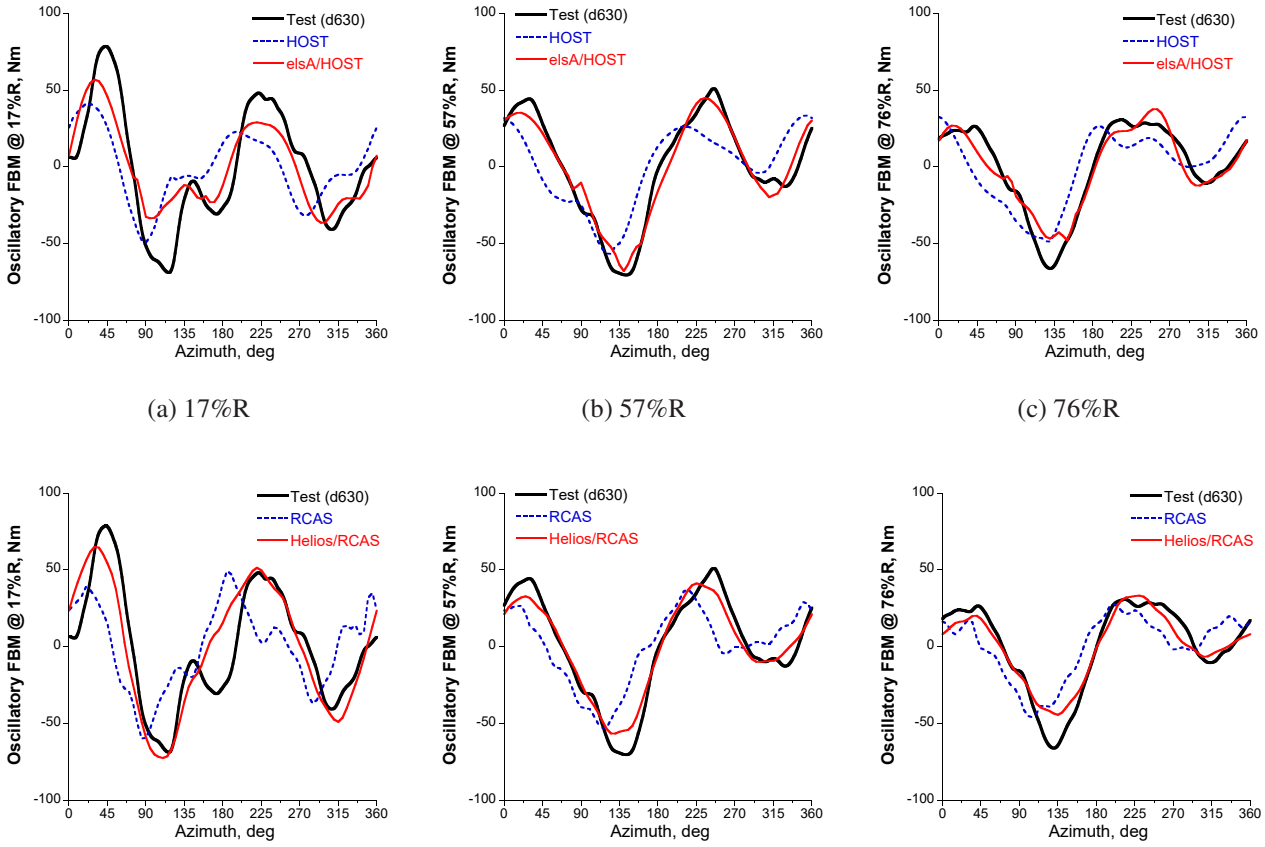

(a) 17%R (b) 57%R (c) 76%R

(d) 17%R (e) 57%R (f) 76%R

Fig. 9. Blade oscillatory flap bending moment.

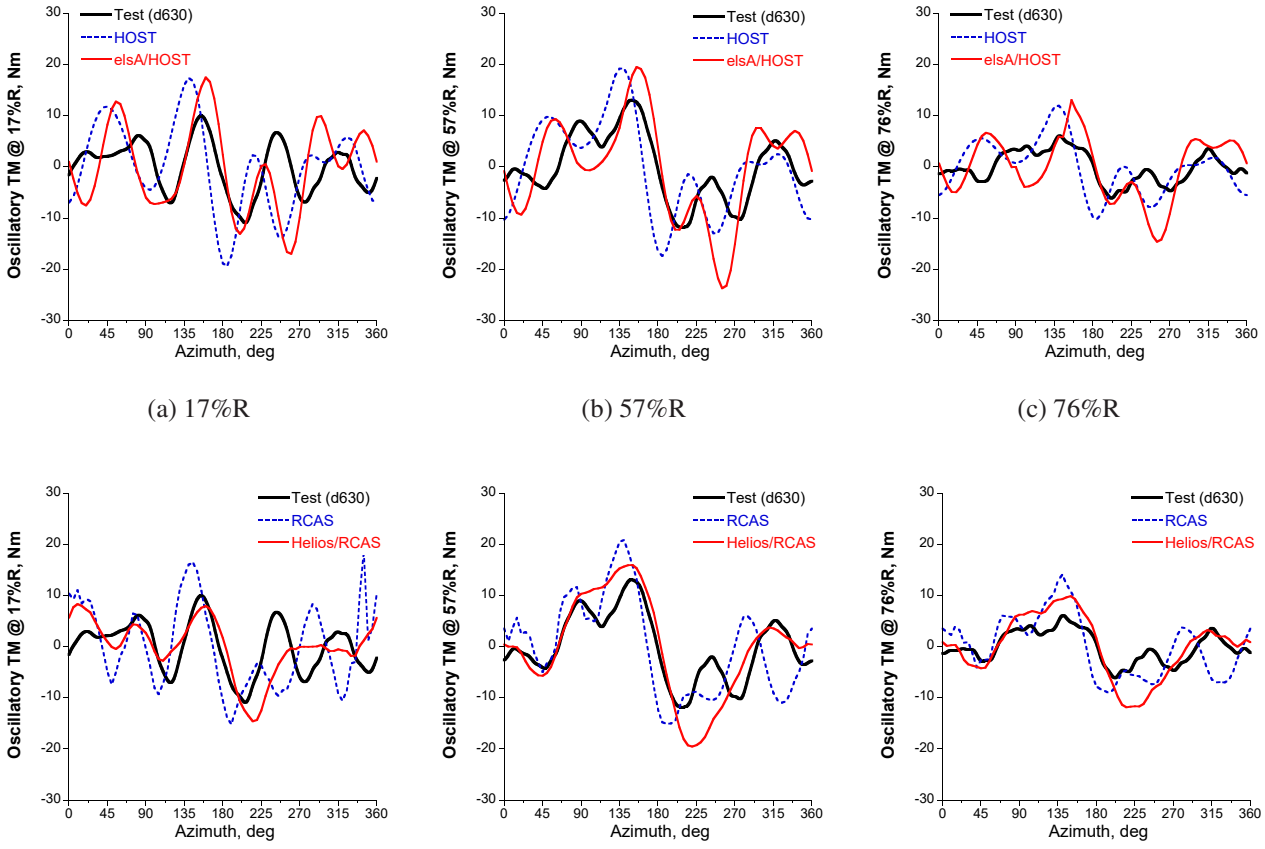

(a) 17%R (b) 57%R (c) 76%R

(d) 17%R (e) 57%R (f) 76%R

Fig. 10. Blade oscillatory torsion moment.

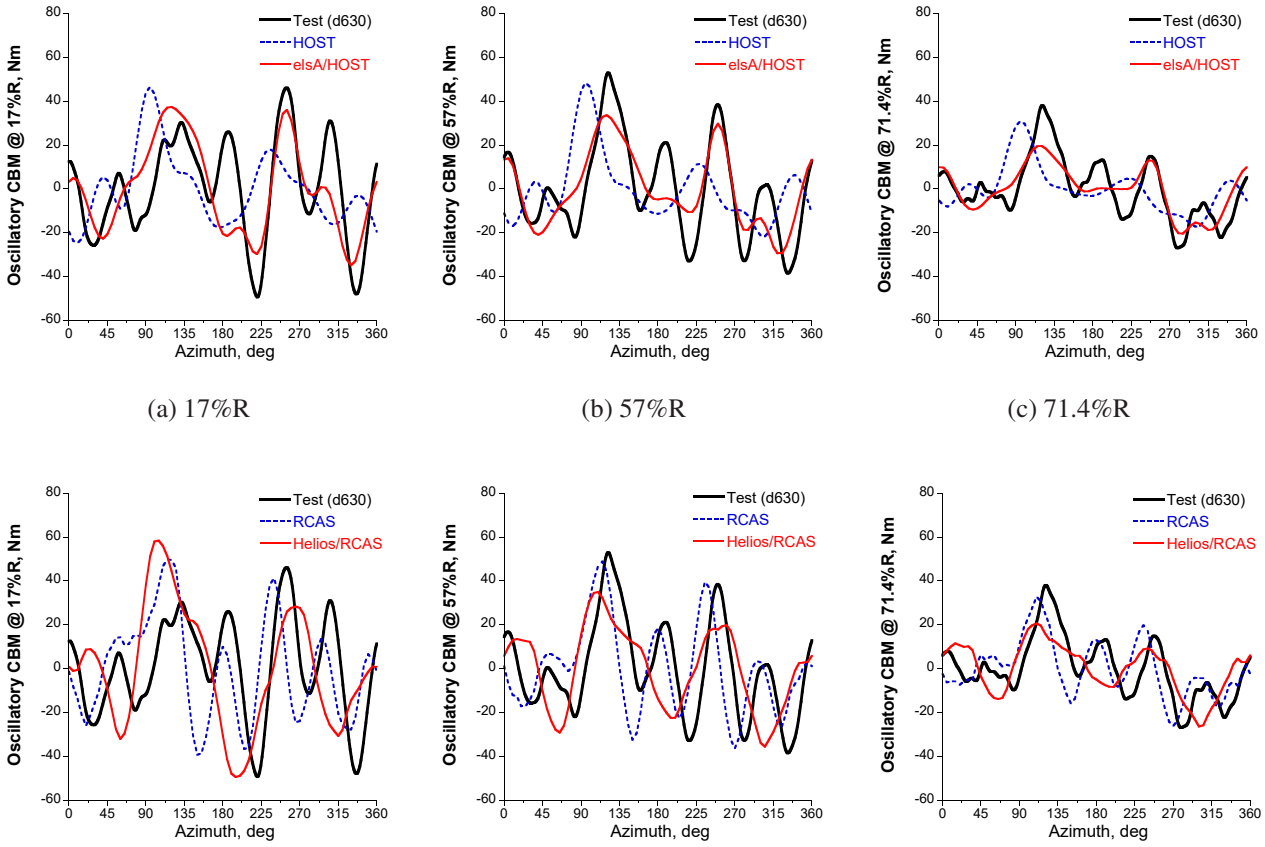

(a) 17%R (b) 57%R (c) 71.4%R

(d) 17%R (e) 57%R (f) 71.4%R

Fig. 11. Blade oscillatory chord bending moment.

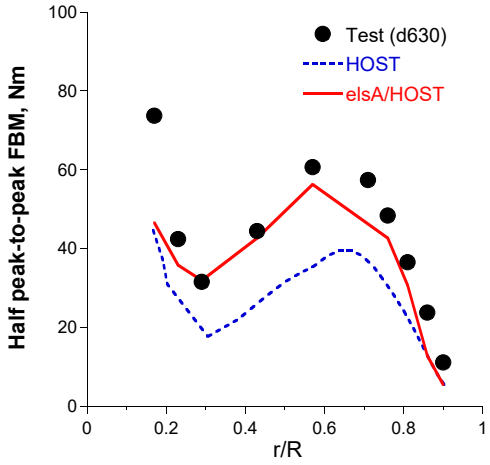

(a) Flap bending moment

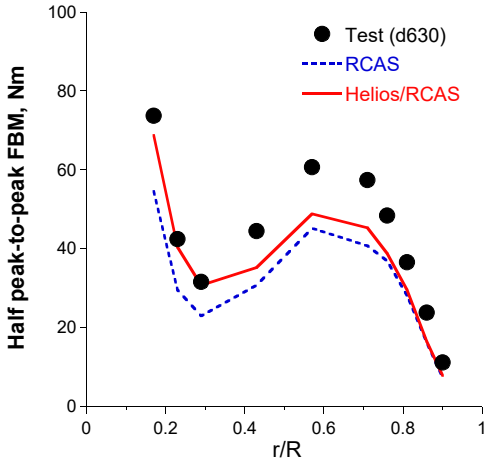

(b) Flap bending moment

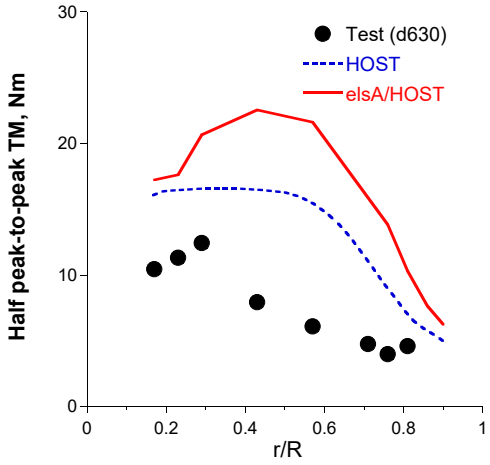

(c) Torsion moment

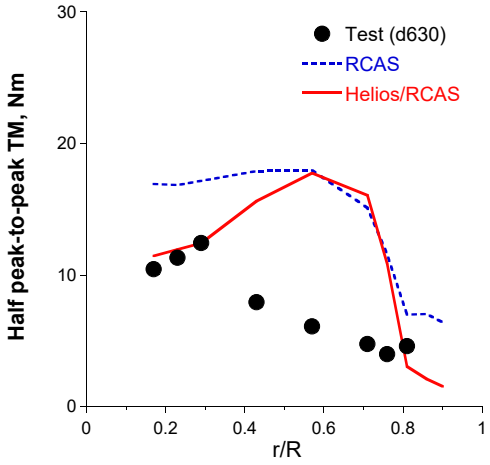

(d) Torsion moment

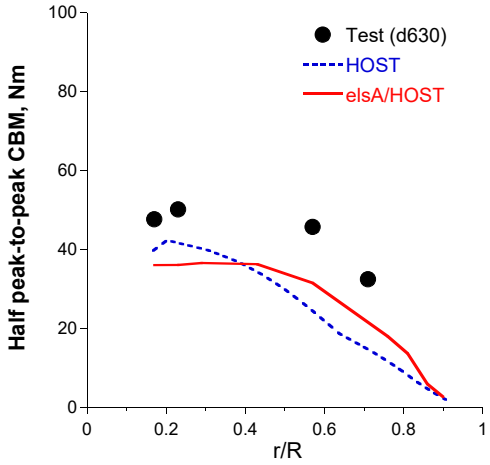

(e) Chord bending moment

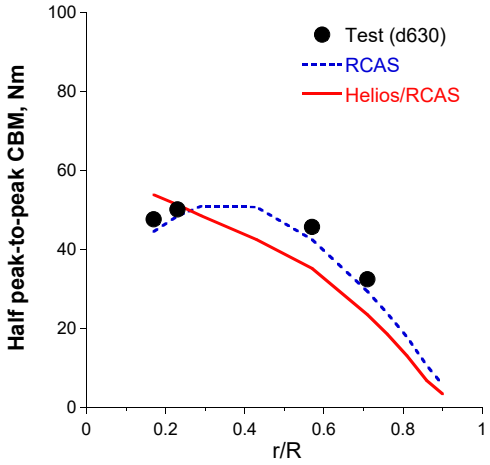

(f) Flap bending moment

Fig. 12. Half peak-to-peak magnitude of blade structural loads.

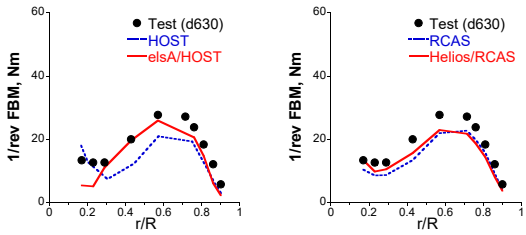

(a) 1/rev magnitude

(b) 1/rev magnitude

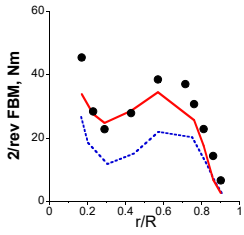

(c) 2/rev magnitude

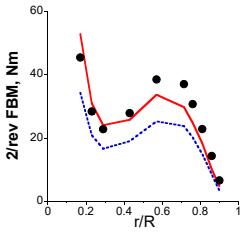

(d) 2/rev magnitude

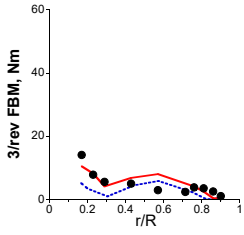

(e) 3/rev magnitude

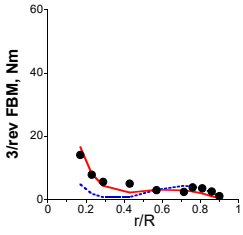

(f) 3/rev magnitude

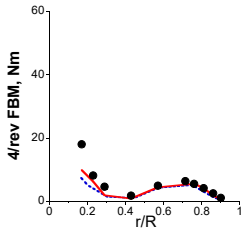

(g) 4/rev magnitude

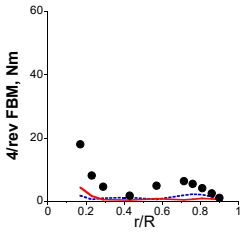

(h) 4/rev magnitude

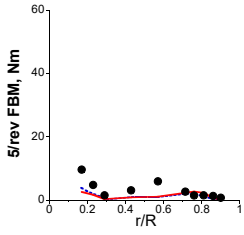

(i) 5/rev magnitude

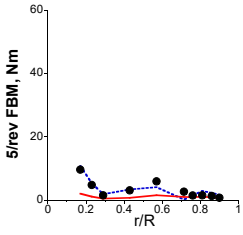

(j) 5/rev magnitude

Fig. 13. Harmonic magnitude of flap bending moment.

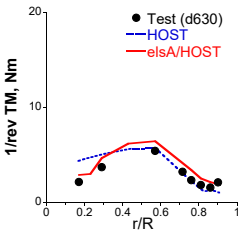

(a) 1/rev magnitude

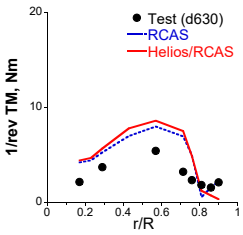

(b) 1/rev magnitude

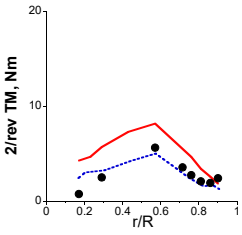

(c) 2/rev magnitude

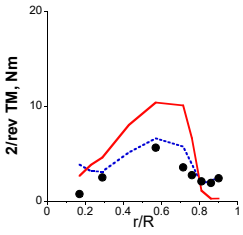

(d) 2/rev magnitude

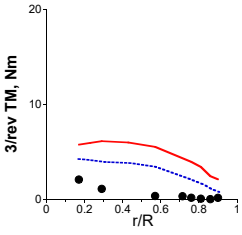

(e) 3/rev magnitude

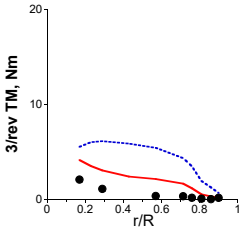

(f) 3/rev magnitude

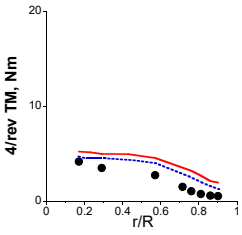

(g) 4/rev magnitude

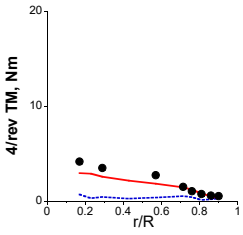

(h) 4/rev magnitude

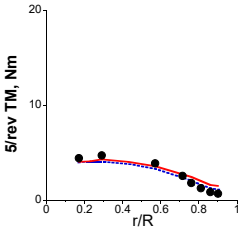

(i) 5/rev magnitude

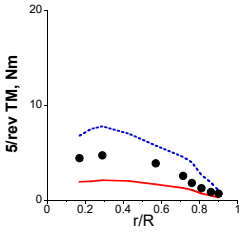

(j) 5/rev magnitude

Fig. 14. Harmonic magnitude of torsion moment.

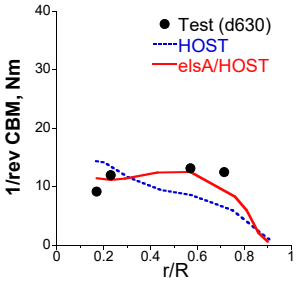

(a) 1/rev magnitude

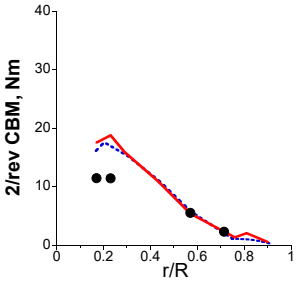

(b) 2/rev magnitude

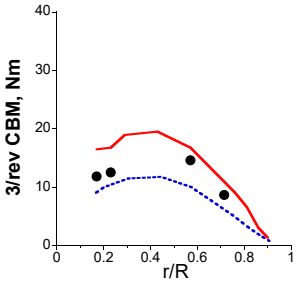

(c) 3/rev magnitude

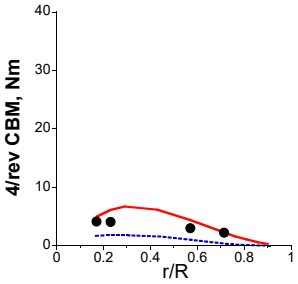

(d) 4/rev magnitude

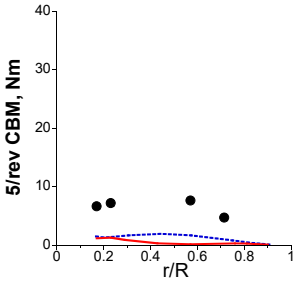

(e) 5/rev magnitude

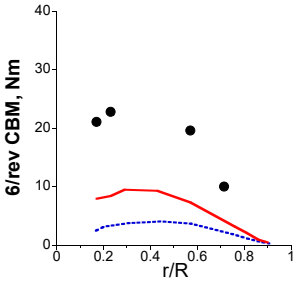

(f) 6/rev magnitude

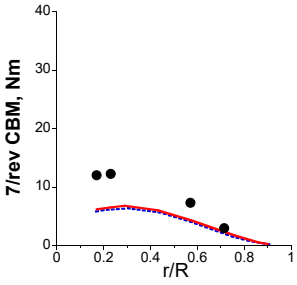

(g) 7/rev magnitude

Fig. 15. Harmonic magnitude of chord bending moment for HOST and elsA/HOST.

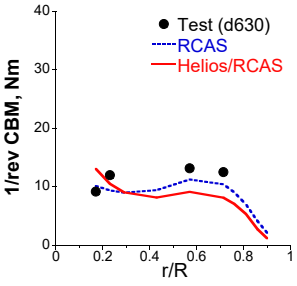

(a) 1/rev magnitude

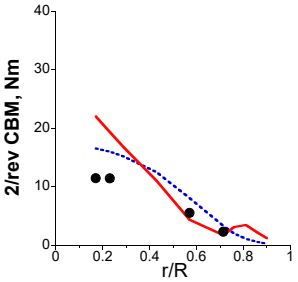

(b) 2/rev magnitude

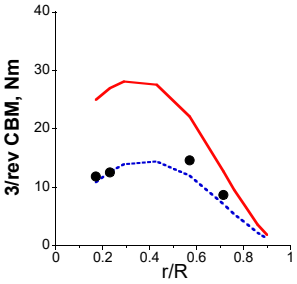

(c) 3/rev magnitude

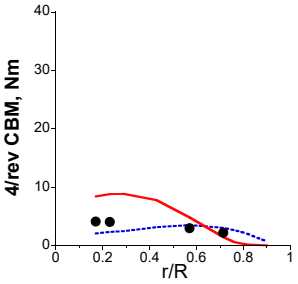

(d) 4/rev magnitude

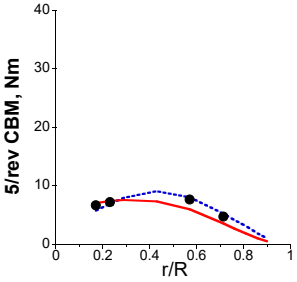

(e) 5/rev magnitude

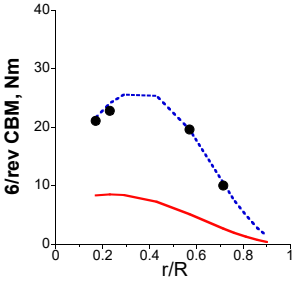

(f) 6/rev magnitude

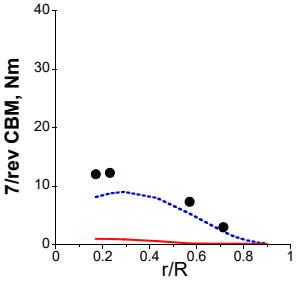

(g) 7/rev magnitude

Fig. 16. Harmonic magnitude of chord bending moment for RCAS and Helios/RCAS.